Double Dielectric-Slab-Filled Waveguide Phase Shifter

FRITZ ARNDT, SENIOR MEMBER, IEEE, ANDREAS FRYE, MANFRED WELLNITZ, AND RAINER WIRSING

Abstract—**A field theory method based on the orthogonal expansion into eigenmodes is presented for the design of double dielectric-slab-filled waveguide phase shifters with linearly tapered sections. Prototypes of 90° differential phase shift with reference to a corresponding empty waveguide of the same length achieved typically about ±4° phase error and less than −30-dB input reflection within ±5-percent bandwidth, for WR 102-band (7–11 GHz) through WR 28-band (26.5–40 GHz) waveguides. Design curves for differential phase shifts of 12.25°, 22.5°, 45°, 90°, 180°, and 270° are given. Utilizing the differential phase compensation effect of the dispersive behavior of the dielectric-filled and empty reference waveguides, the phase error is only ±1° within ±8.5-percent bandwidth. Further investigations include composite phase shifters, mechanical lateral displacement, and tolerance influences. An experimental 90° phase shifter for 14-GHz midband frequency shows good agreement between theory and measurements.**

I. Introduction

DIELECTRIC-SLAB loading of rectangular waveguides [1]–[7] is a well-known technique to build simple but effective differential phase shifters. In a previous paper [8], an exact field theory design has been introduced for multisection impedance-matched single-slab structures. This type may be applied especially for a mechanically adjustable phase shift where, besides appropriate impedance matching, a sufficient differential phase shift range (e.g., 0°–360°) as a function of mechanical displacement is required.

In this paper, a double dielectric-slab-filled waveguide (Fig. 1) is investigated with a preferably fixed dielectric. A nearly constant differential phase shift (e.g., 90° ± 4°) in relation to an empty reference waveguide is required within a certain frequency range (e.g., 10-percent bandwidth). Possible applications exist in the field of antenna beamforming networks where often a combination of hybrids and fixed phase shifters is used. Since, as for all antenna applications, low input VSWR is required, the dielectric slabs are positioned in regions of low TE_{m0} wave electric-field intensity, at the sidewalls of the waveguide (Fig. 1). This may also help to meet associated power specifications. Tapered matching sections are provided, which are taken to be linear for ease of fabrication. Because the dielectric can be fastened to the waveguide sidewalls by special adhesives (for instance, with a styrol polymerisate compound base ($\epsilon_r = 2.54$)), this type of phase shifter also has good mechanical stability.

Manuscript received February 13, 1984; revised December 7, 1984.

The authors are with the Microwave Department, University of Bremen, Kufsteiner Strasse, NW 1, D-2800 Bremen 33, West Germany.

A field theory method using the orthogonal expansion [8] in suitable eigenmodes is presented for the design of such phase shifters. This allows direct calculation of the scattering matrix and the immediate inclusion of higher order mode coupling along the three-dimensional structure. Prototypes for some often used frequency bands, for rectangular and square waveguide sidewalls, are calculated. Phase shifter designs for waveguide dimensions and frequencies other than the prototype values considered can be obtained using the simple scaling relations given. The deviations from the exact design may be tolerable for many practical applications.

Extreme broad-band behavior of the differential phase shift is possible by utilizing the differential phase compensation effect resulting from the different dispersion characteristics of the waveguide with and without the dielectric in the vicinity of the empty guide TE_{10} cutoff frequency. Compared with the well-known periodic loading principle which is used for square waveguide circular polarizers [9], the continuously loaded structure of Fig. 1 has the advantage of yielding low input VSWR without ripples as a function of frequency.

II. Theory

The linearly tapered structure (Fig. 1) is approximated by a stepped transition (cf. Fig. 2(a)) with a hundred steps at each side. The basic configuration for the field theory treatment, the five-layer section of finite length (Fig. 2(b)), includes the general case of asymmetrical displacement of the dielectric slabs which may be taken into account for mechanically adjustable phase shifters or for test calculations.

As in [8], for each subregion, $\nu = \mathrm{I}$ to VI (Fig. 2(b)), the fields [2] of the resulting TE_{n0} wave (if a TE_{m0} wave is incident)

$$\vec{E}^{(\nu)} = -j\omega\mu\nabla \times \vec{\Pi}_{hx}^{(\nu)} \quad \vec{H} = \nabla \times \nabla \times \vec{\Pi}_{hx}^{(\nu)} \qquad (1)$$

are derived from the x-component of the magnetic Hertzian vector potential $\vec{\Pi}_h$, which may be approximately expressed as the sum of N eigenmodes satisfying the vector Helmholtz equation and the boundary condition $E_y = 0$ at $x = 0$. The accuracy of the approximation improves as N increases.

For the calculation of the mutual relations of the field amplitude coefficients along the five-layer section, and to

0018-9480/85/0500-0373$01.00 ©1985 IEEE

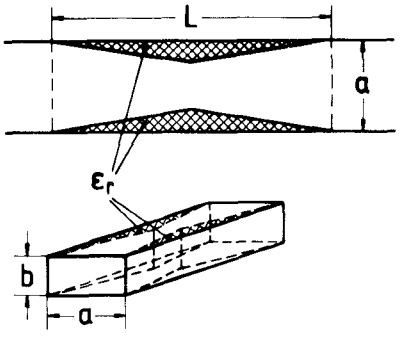

Fig. 1. Double dielectric-slab-filled waveguide phase shifter tapered for the entire length.

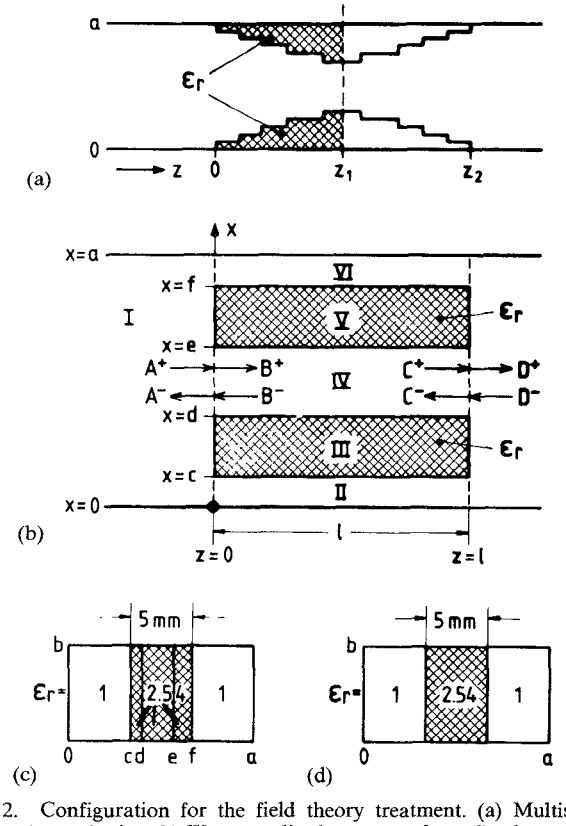

Fig. 2. Configuration for the field theory treatment. (a) Multisection step discontinuity. (b) Wave amplitude vectors of one five-layer section of finite length. (c) Five-layer cross section. (d) Three-layer cross section [8] compared with (c) for test purposes (waveguide housing dimensions $a = 15.799$ mm, $b = 7.899$ mm).

determine the common propagation constant k_z, the Hertzian vector potentials in the subregions $\nu = \mathrm{II}, \cdots, \mathrm{VI}$ are assumed to be

$$\Pi_{hx}^{(\mathrm{II})} = \sum_{n=1}^{N} V_n^{(\mathrm{II})} \sin\left(k_{xn}^{(\mathrm{II})} x\right) e^{-jk_{zn}z} \tag{2}$$

$$\Pi_{hx}^{(s)} = \sum_{n=1}^{N} \left[V_n^{(s)} \sin\left(k_{xn}^{(s)} x\right) + W_n^{(s)} \cos\left(k_{xn}^{(s)} x\right)\right] e^{-jk_{zn}z} \tag{3}$$

with $s = \mathrm{III}, \cdots, \mathrm{VI}$.

The propagation constants for the eigenmodes in the empty guide ($\nu = I$), $k_{zn}^{(I)}$, and the dielectric-filled guide ($\nu = \mathrm{II}, \cdots, \mathrm{VI}$), k_{zn}, are

$$k_{zn}^{(\mathrm{I})2} = \omega^2 \mu_0 \epsilon_0 - \left(\frac{n\pi}{a}\right)^2 \qquad k_{zn}^2 = \omega^2 \mu_0 \epsilon_0 \epsilon_r^{(\nu)} - k_{xn}^{(\nu)2} \tag{4}$$

for $\nu = \mathrm{II}, \cdots, \mathrm{VI}$.

k_{zn} is determined via field matching [2] of the transversal field components H_z and E_y along the boundaries at $x = c, d, e, f$. The requirements of the system determinant of the related matrix equation (cf. Appendix) to be zero results in a transcendental equation for k_{zn}, which is solved numerically. The boundary condition $E_y = 0$ at $x = a$ is satisfied by the condition $W_n^{(\mathrm{VI})} = -V_n^{(\mathrm{VI})} \tan(k_{xn}^{(\mathrm{VI})} a)$.

For calculation of the scattering matrix at the step discontinuity at $z = 0$ (Fig. 2(b)) in (2) and (3), the expression $\exp(-jk_{zn}z)$ has to be replaced by the expressions of the forward (+) *and* backward (−) eigenwaves: $[B_n^+ \cdot \exp(-jk_{zn}z) + B_n^- \cdot \exp(jk_{zn}z)]$. The Hertzian vector potential in the empty subregion I is assumed to be

$$\Pi_{hx}^{(\mathrm{I})} = \sum_{n=1}^{N} V_n^{(\mathrm{I})} \sin\left(\frac{n\pi}{a} x\right) \cdot \left[A_n^+ \cdot \exp\left(-jk_{zn}^{(\mathrm{I})} z\right) + A_n^- \cdot \exp\left(+jk_{zn}^{(\mathrm{I})} z\right)\right]. \tag{5}$$

By matching the transversal field components E_y and H_x at the corresponding interfaces of the adjacent subregions (Fig. 2(b)) at $z = 0$ and using the orthogonal property of the modes [2], the coefficients A_n^+, A_n^-, B_n^+, and B_n^- can be related to each other with the equation

$$\begin{aligned} \frac{a}{2} \cdot V_n^{(\mathrm{I})} \cdot k_{zn}^{(\mathrm{I})} \cdot \left(A_n^+ - A_n^-\right) &= \sum_{m=1}^{N} \Big\{ V_m^{(\mathrm{II})} I_{1nm}^{(\mathrm{II})} + V_m^{(\mathrm{III})} I_{1nm}^{(\mathrm{III})} + W_m^{(\mathrm{III})} I_{2nm}^{(\mathrm{III})} \\ &\quad + V_m^{(\mathrm{IV})} I_{1nm}^{(\mathrm{IV})} + W_m^{(\mathrm{IV})} I_{2nm}^{(\mathrm{IV})} + V_m^{(\mathrm{V})} I_{1nm}^{(\mathrm{V})} \\ &\quad + W_m^{(\mathrm{V})} I_{2nm}^{(\mathrm{V})} + V_m^{(\mathrm{VI})} \left(I_{1nm}^{(\mathrm{VI})} - I_{2nm}^{(\mathrm{VI})}\right) \Big\} k_{zm} \\ &\quad \cdot \left(B_m^+ - B_m^-\right) \end{aligned} \tag{6}$$

or abbreviated

$$\left(N_E\right)_{nn} \left(A_n^+ - A_n^-\right) = \sum_{m=1}^{N} \left\{\left(M_E\right)_{nm}\right\} \left(B_m^+ - B_m^-\right) \tag{6a}$$

and with

$$\frac{a}{2} \cdot V_n^{(\mathrm{I})} \cdot k_{zn}^{(\mathrm{I})2} \cdot \left(A_n^+ + A_n^-\right) = \sum_{m=1}^{N} \left\{\left(M_E\right)_{nm} \cdot k_{zm}\right\} \left(B_m^+ + B_m^-\right) \tag{7}$$

or abbreviated

$$\left(N_H\right)_{nn} \left(A_n^+ + A_n^-\right) = \sum_{m=1}^{N} \left\{\left(M_H\right)_{nm}\right\} \left(B_m^+ + B_m^-\right) \tag{7a}$$

where the $I_{1nm}^{(\nu)}$ and $I_{2nm}^{(\nu)}$ are the coupling integrals given in the Appendix.

Equations (6a) and (7a), written as matrix equations, lead directly to the scattering matrix at $z = 0$

$$\begin{pmatrix} (A)^- \\ (B)^+ \end{pmatrix} = \begin{pmatrix} (S_{11}) & (S_{12}) \\ (S_{21}) & (S_{22}) \end{pmatrix} \begin{pmatrix} (A)^+ \\ (B)^- \end{pmatrix} \tag{8}$$

where (S_{11}), (S_{12}), (S_{21}), and (S_{22}) are also given in the Appendix.

At the step discontinuity at $z = l$ (Fig. 2(b)), the scattering matrix (S) of (9) still holds for inverted wave-amplitude vectors

$$\begin{pmatrix} (D)^+ \\ (C)^- \end{pmatrix} = (S) \begin{pmatrix} (D)^- \\ (C)^+ \end{pmatrix}. \tag{9}$$

For the calculation of the scattering matrix $(S)_l$ of the total double dielectric-slab-filled structure (Fig. 2(b)) of length l

$$\begin{pmatrix} (A)^- \\ (D)^+ \end{pmatrix} = \begin{pmatrix} (S_{11})_l & (S_{12})_l \\ (S_{21})_l & (S_{22})_l \end{pmatrix} \cdot \begin{pmatrix} (A)^+ \\ (D)^- \end{pmatrix} \tag{10}$$

the relations between the wave-amplitudes along the corresponding intermediate waveguide section have to be taken into account

$$(B)^- = (R)(C)^- \quad (C)^+ = (R)(B)^+$$

where $R_{mm} = e^{-jk_{zm} \cdot l}$ (diagonal matrix of the waveguide section between the two discontinuities). The scattering coefficients of (10) are then obtained analogously to [8, eq. (4)].

The series connection of two structures with the scattering matrices $(S)^{(1)}$ and $(S)^{(2)}$ is calculated by direct combination [11] of the scattering elements. Opposite to the common treatment with transmission matrices, this procedure preserves numerical accuracy and avoids the hitherto known numerical instabilities due to resonance and interference effects of higher order modes, since the expressions contain exponential functions with only negative arguments. The scattering coefficients for two series-connected structures are given in the Appendix. The scattering matrix for more structures is found analogously using (A5) iteratively.

For the computer analysis, the inclusion of only five eigenmodes ($N = 5$ in (2)–(7), and of only three modes for the symmetrical cases, since the n-even modes do not enter) has turned out to yield sufficient asymptotic behavior (within drawing accuracy) of the calculated results, as has been ascertained by considering up to twenty eigenmodes. Further, tests were performed by comparing propagation constants for various modes at various frequencies calculated for the same cross-section structure by means of different versions of realization. As a typical example, the normalized propagation constants k_z/k_0 (k_0 = free-space wavenumber) of the TE_{100} mode at 15 GHz are: $k_z/k_0 = -j6.204328$ for $c = 5.3995$ mm, $d = 6.000$ mm, $e = 9.000$ mm, $f = 10.399$ mm, $\epsilon_r^{(III)} = \epsilon_r^{(IV)} = \epsilon_r^{(V)} = 2.54$ (cf. Fig. 2(c)), and $k_z/k_0 = -j6.204329$ for the analogous one-slab structure (cf. Fig. 2(d)) calculated by the computer program of [8] ($a = 15.799$ mm, $b = 7.899$ mm).

TABLE I
MAXIMUM DIELECTRIC-SLAB WIDTH D IN MILLIMETERS FOR WR 90 AND WR 62 (X- AND Ku-BAND) PHASE SHIFTERS FOR 45°, 90°, 180°, 270° MIDBAND DIFFERENTIAL PHASE SHIFT

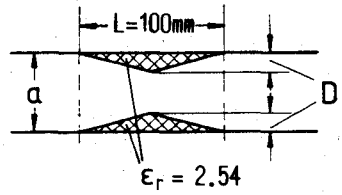

Frequency band waveguide dimensions	Midband frequency f_0 (GHz)	Midband differential phase shift * (°)	Width of dielectric slab D (mm)	Maximummm phase error within ± 5 % bandwidth (°)	Maximum input reflection within ± 5 % bandwidth (dB)
WR 90 (X-band) a = 22.86 mm b = 10.16 mm	9	45	5.00	-0.6, +1.1	- 28.4
		90	6.46	-1.8, +2.7	- 27.7
		180	8.75	-5.5, +4	- 30
		270	10.858	-7.7, +5.9	- 28.8
	10	45	4.89	-1.6, +2	- 31.6
		90	6.282	-3.6, +4.3	- 30.7
		180	8.44	-7.1, +8.2	- 32.8
		270	10.445	-11, +9.7	- 30.2
WR 62 (Ku-band) a = 15.799mm b = 7.899mm	12	45	3.05	-0.08, +1	- 30
		90	3.91	-1.1, +0.6	- 28.8
		180	5.16	-0.5, +2.3	- 31
		270	6.24	-0.3, +3.9	- 30.2
	14	45	3.01	-1.2, +1.6	- 35.5
		90	3.82	-2.9, +3.7	- 33
		180	5.00	-6.3, +7.7	- 33.7
		270	6.01	-9.2, +11	- 37.2
	15	45	2.97	-1.7, +2	- 37.3
		90	3.74	-4, +4.6	- 34.7
		180	4.86	-8.2, +9.5	- 34.8
		270	5.83	-11.8, +13.4	- 36.2
	16	45	2.91	-2.1, +2.5	- 38.8
		90	3.65	-4.8, +5.5	- 36.1
		180	4.73	-9.9, +11	- 36.3
		270	5.655	-14, +15.6	- 37.4
	18	45	2.78	-2.7, +3.1	- 41.2
		90	3.47	-6.2, +7	- 38.3
		180	4.44	-12.6, +14	- 38.1
		270	5.275	-17.8, +19.3	- 39.4

*with reference to a corresponding empty waveguide of same length.

Dielectric material: Rexolite (styrol polymerisate compound) $\epsilon_r = 2.54$, $\tan\delta = 6.6 \cdot 10^{-4}$ (25°C, 10 GHz).

Since the coupling integrals (see Appendix) may be solved by direct integration, and symmetry conditions (Fig. 2(a)) may be included, the computing time is only about 6 min for a total set of scattering parameters as a function of frequency for one design example (Siemens 7880 computer of the University of Bremen).

III. RESULTS

In Table I, the maximum dielectric slab width D is given for phase shifters in WR 90 (X-), and WR 62 (Ku-band) waveguides, with 45°, 90°, 180°, and 270° midband differential phase shift, respectively, referred to a corresponding empty waveguide. The length of the dielectric slab section in these examples is chosen to be $L = 100$ mm as a compromise between size and length requirements for a

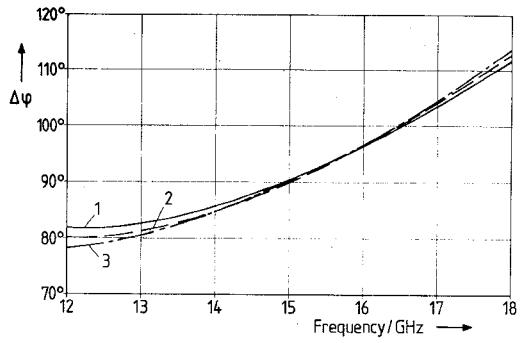

(a)

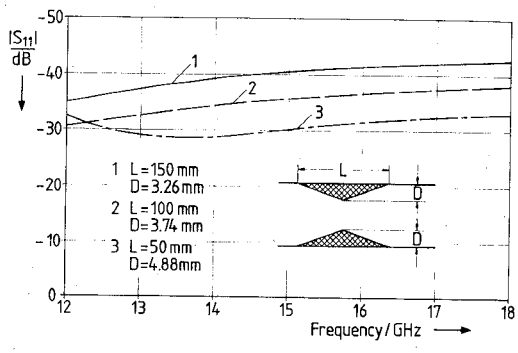

(b)

Fig. 3. 90°-WR 62 (*Ku*)-band phase shifter ($f_0 = 15$ GHz) with dielectric length L as a parameter (dimensions cf. Table I). (a) Differential phase shift $\Delta\varphi$ as a function of frequency. (b) Input reflection coefficients $|S_{11}|$ in decibels.

given maximum input reflection value (about -30 dB). Rexolite (Styrol Polymerisate Compound, $\epsilon_r = 2.54$, $\tan\delta = 6.6 \cdot 10^{-4}$ (25°C, 10 GHz)) has been selected for the dielectric material because it is relatively easy to handle mechanically.

To demonstrate the influence of the dielectric slab length L, Fig. 3(b) shows the input reflection coefficients $|S_{11}|$ in decibels as a function of frequency for three lengths $L = 50$ mm, $L = 100$ mm, and $L = 150$ mm as the parameters. As expected, the best input reflection behavior is provided by $L = 150$ mm (curve 1). The differential phase shift (Fig. 3(a)) is less influenced by length variation.

In Table II, the maximum dielectric slab width D is calculated for WR 62, WR 42, and WR 28 (*Ku*-, *K*-, and *Ka*-band) phase shifters with 90° midband differential phase shift and for different lengths L of the dielectric slab section (L is about 2.5 λ_0, 5 λ_0, and 7.5 λ_0. λ_0 = free-space wavelength at midband frequency). For L about 7.5 λ_0, the phase errors are less than $\pm 4°$ and the maximum input reflection is less than -38 dB for a ± 5-percent frequency variation around the midband frequency. Included also is a 90° phase shifter for a square *Ku*-band waveguide showing exactly the same behavior (for the TE_{10} incident wave) as its rectangular counterpart.

For the practical design of phase shifters with a desired differential phase shift $\Delta\varphi$ for a desired midband frequency, $f_0/f_{\text{cutoff empty}}$ (normalized to the TE_{10} cutoff frequency of the empty waveguide), Fig. 4 shows the normalized maximum width D/a of the linearly tapered double dielectric

TABLE II
MAXIMUM DIELECTRIC SLAB WIDTH D IN MILLIMETERS FOR 90° WR 62-, WR 42-, AND WR 28-(*Ku*-, *K*-, AND *Ka*-BAND) PHASE SHIFTERS WITH DIFFERENT DIELECTRIC SLAB LENGTH L (ABOUT 2.5 λ_0, 5 λ_0, 7.5 λ_0, λ_0 = FREE-SPACE MIDBAND WAVELENGTH)

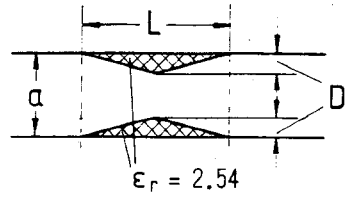

Frequency band waveguide dimensions	Midband frequency f_0 (GHz)	Length of dielectric L (mm)	Width of dielectric slab D (mm)	Maximum phase error within ± 5 % bandwidth (°)	Maximum input reflection within ± 5 % bandwidth (dB)
WR 62 (Ku-band) a = 15.799mm b = 15.799mm	14	50	5.00	-3.5, +4	- 29
		100	3.82	-2.9, +3.7	- 33
		150	3.32	-2, +4	- 38
WR 62 (Ku-band) a = 15.799mm b = 7.899mm	14	50	5.00	-3.5, +4	- 29
		150	3.32	-2, +4	- 38
WR 42 (K-band) a = 10.67 mm b = 5.335mm	22	32	3.37	-5, +4	- 29
		64	2.58	-4, +4	- 34
		96	2.24	-4, +4	- 38
WR 28 (Ka-band) a = 7.11 mm b = 3.55 mm	33	21	2.25	-6, +3	- 29
		42	1.72	-5, +3	- 34
		63	1.49	-2.5, +1.5	- 38

*with reference to a corresponding empty waveguide of same length.
Dielectric material: Rexolite (cf. Table I).

slab (a = waveguide width) for two values of normalized length L/a. The longer version ($g = 100$) yields an input reflection coefficient of about -30 dB for about 10-percent bandwidth, the shorter one of about -27 dB. The curves are the condensed result of a large number of design data and have been checked from the WR 90 (*X*-band) to the WR 28 (*Ka*-band) frequency range (8.2 to 40 GHz). The maximum deviations of the phase shift of phase shifters designed with Fig. 4 against the directly designed prototypes are about ± 0.5 percent. The error in the input reflection coefficient is negligible.

By utilizing the differential phase compensation effect of the dispersive behaviors of the dielectric-filled and empty reference waveguide, extreme broad-band behavior of the differential phase shift is possible. Fig. 5 (solid lines) presents the resulting differential phase shift and input reflection curves of a 90° phase shifter within a WR 102 waveguide housing ($a = 25.908$ mm, $b = 12.954$ mm). The phase error is only $\pm 1°$ between 6.9 and 8.2 GHz. For comparison, a periodic five-iris-loaded square waveguide polarizer [9] has been calculated with the orthogonal expansion method for corrugated structures [12]. The results

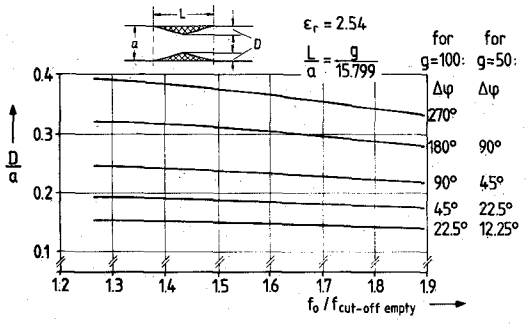

Fig. 4. Curves for the practical design of double dielectric-slab-filled phase shifters. Maximum width D normalized to the width a of the waveguide as a function of the desired midband frequency f_0 normalized to the empty waveguide TE_{10} cutoff frequency. Parameter is the desired differential phase shift $\Delta\varphi$ for two values of normalized lengths L/a (e.g., for the *Ku*-band waveguide with $a = 15.799$ mm: $L = 100$ mm and 50 mm). The dielectric material is Rexolite ($\epsilon_r = 2.54$), cf. Table I.

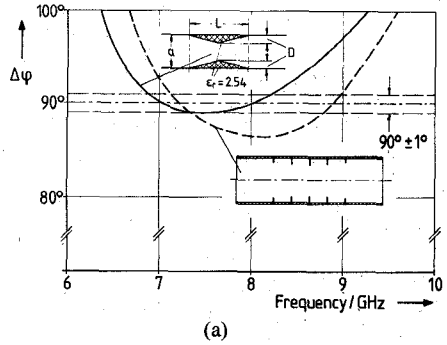

(a)

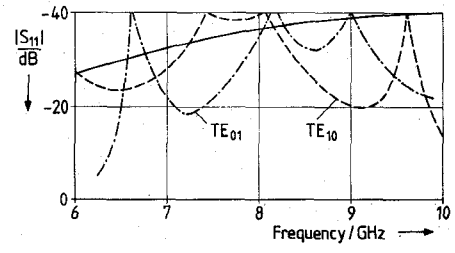

(b)

Fig. 5. 90° double dielectric-slab-filled phase shifter with broad-band differential phase shift (solid line) (waveguide dimensions $a = 25.908$ mm, $b = 12.954$ mm (WR 102), $D = 5.643$ mm, $L = 229.6$ mm) compared with a periodic iris-loaded square waveguide phase shifter [9] (dashed line, dashed–dotted line) calculated with the method in [12]. (a) Differential phase shift $\Delta\varphi$. (b) Input reflection coefficient $|S_{11}|$ in decibels (for the periodic loaded phase shifter: TE_{01} wave, or TE_{10} wave incident, respectively).

are presented also in Fig. 5 (dashed, and dashed–dotted lines). The continuously dielectric-loaded structure designed has the advantage of yielding low input reflection without ripples as a function of frequency. It should be pointed out that the iris-loaded polarizer in [9] utilizes the differential phase shift of orthogonal TE_{10} and TE_{01} modes within the *same* square waveguide, whereas the TE_{10} mode differential phase shift of the dielectric-slab-filled rectangular waveguide phase shifter investigated in this paper is related to an empty rectangular reference waveguide of the same length and dimensions. Such relative phase shift requirements are usually needed for antenna beam forming

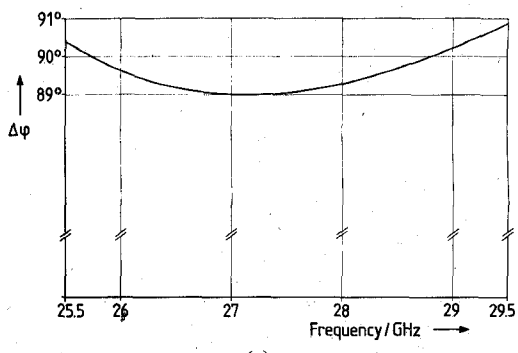

(a)

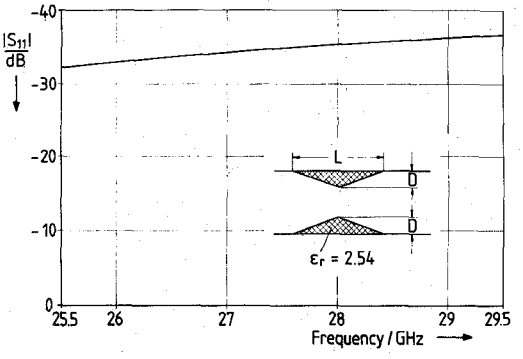

(b)

Fig. 6. WR 28 (*Ka*)-band 90° phase shifter with broad-band differential phase shift (waveguide dimensions $a = 7.112$ mm, $b = 3.556$ mm, $D = 1.549$ mm, $L = 63$ mm). (a) Differential phase shift $\Delta\varphi$. (b) Input reflection coefficeint $|S_{11}|$ in decibels.

networks (cf., e.g., [13]). Moreover, periodic loading, which [9] employs, may not be considered as an approximation to the continuous loading since the discrete susceptances assumed there become invalid because of the mutual interaction of the evanescent modes excited at the discontinuities when they are placed close together.

Fig. 6 shows the differential phase shift and the input reflection coefficient of a second design example, for a WR 28 (*Ka*-band, 26.5–40 GHz) waveguide ($a = 7.112$ mm, $b = 3.556$ mm). Further design data are given in Table III. For the practical design of $90° \pm 1°$ differential phase compensated phase shifters with desired midband frequencies other than given in Table III, the approximate relations for the normalized maximum width $D/a \approx 0.218$ and normalized length $L/a \approx 0.886$ may be applied where the width a of the waveguide housing is given by $a/\lambda_0 \approx 0.64$ (λ_0 is the free-space wavelength at the desired midband frequency f_0).

The calculated phase shifters can be cascaded to construct phase shifters with increased overall differential phase shift. This is illustrated in Fig. 7 where a 90° phase shifter (2) is composed of three 30° phase shifters (1). The comparison with the direct 90° phase-shifter-type (3) indicates that the differential phase behavior is nearly the same, while the input reflection coefficient is higher because of the greater number of discontinuities.

Further, the input reflection coefficient and the phase shift were calculated as a function of the lateral displace-

TABLE III
DESIGN DATA FOR 90° PHASE SHIFTERS WITH BROAD-BAND DIFFERENTIAL PHASE SHIFT

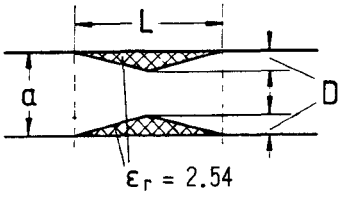

$\Delta\varphi = 90°$
Midband differential phase shift *

Frequency band waveguide dimensions	Midband frequency f_0 (GHz)	Length of dielectric L (mm)	Width of dielectric slab D (mm)	Maximum phase error within ±8.5 % bandwidth (°)	Maximum input reflection (dB)
WR 102 a = 25.908mm b = 12.954mm	7.55	229.6	5.643	±1	- 31
WR 62 (Ku-band) a = 15.799mm b = 7.899mm	12.2	139.95	3.441	±1	- 30
WR 51 a = 12.954mm b = 6.477mm	14.85	114.78	2.821	±1	- 30
WR 34 a = 8.636 mm b = 4.318 mm	22.35	76.8	1.881	±1	- 31
WR 28 (Ka-band) a = 7.112 mm b = 3.556 mm	27.2	63.0	1.549	±1	- 32

*with reference to a corresponding empty waveguide of same length.

ment h of the dielectric slabs for possible applications as a mechanically variable phase shifter, and for the investigation of the tolerance influence of that parameter. The results are shown in Fig. 8 for an example with 14-GHz midband frequency. Up to 530°, differential phase shift is achieved for maximum displacement $h = 3.8995$ mm within the WR 62 (*Ku*-band) waveguide housing, while the input reflection is less than -30 dB. A change of the displacement of about 0.1 mm leads to a differential phase error up to about 7°. This verifies the result of calculations of the influence of geometrical tolerances on the differential phase: the most critical parameter is the maximum width D. A change of this parameter within ± 3 percent leads to a phase error of about triple that value. This fact has to be taken into account if the dielectric is fastened to the waveguide sidewalls by adhesives. The influence on the input reflection coefficient, however, is negligible.

The photograph of a 90° phase-shifter prototype for a 14-GHz midband frequency and with $L = 100$ mm is presented in Fig. 9(a). The maximum width D of the dielectric ($\epsilon_r = 2.54$, Rexolite) is $D = 3.72$ mm (cf. Table I, where

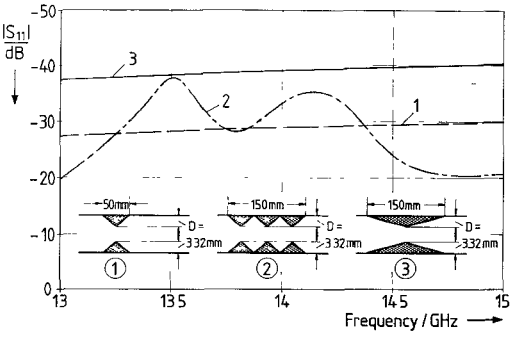

(a)

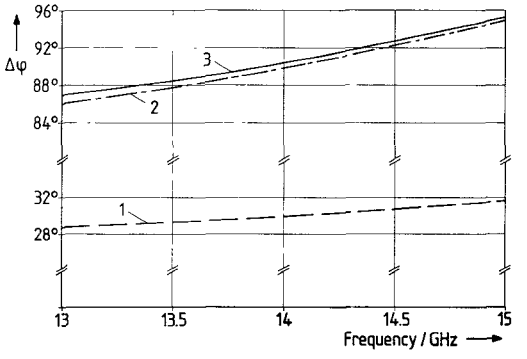

(b)

Fig. 7. WR 62 (*Ku*)-band 90° phase shifter (2) composed of three 30° phase shifters (1) and compared with a 90° phase shifter (3) of the same overall length. (a) Input reflection coefficients $|S_{11}|$ in decibels. (b) Differential phase shift $\Delta\varphi$ as a function of frequency.

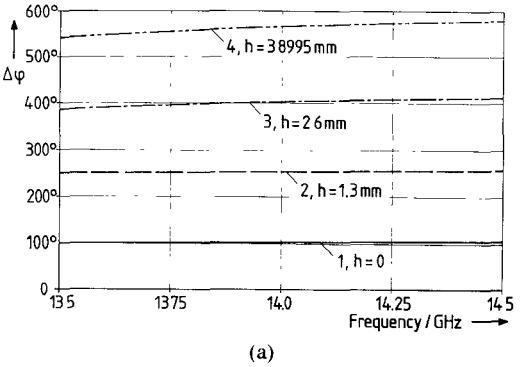

(a)

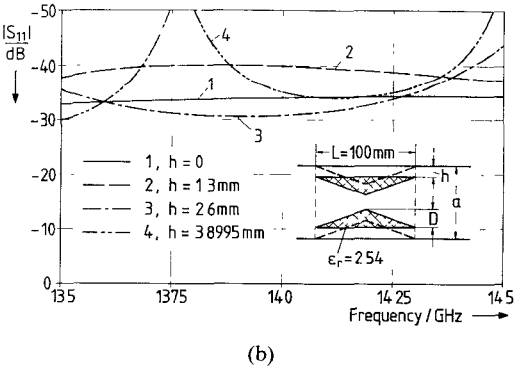

(b)

Fig. 8. WR 62 (*Ku*)-band phase shifter with mechanically variable phase shift as a function of the lateral displacement h. (a) Differential phase shift $\Delta\varphi$ as a function of frequency. (b) Input reflection coefficients $|S_{11}|$ in decibels.

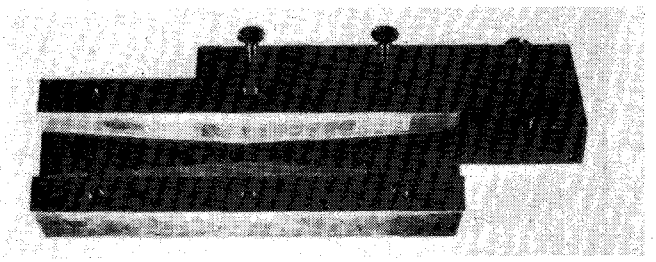

(a)

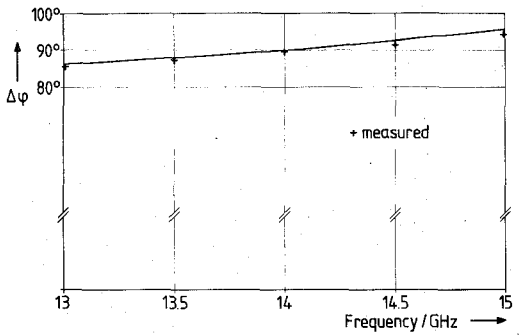

(b)

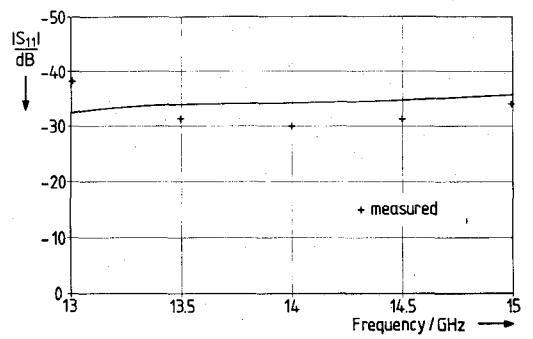

(c)

Fig. 9. Realized 90°-WR 62 (*Ku*)-band phase shifter ($f_0 = 14$ GHz) (dimensions cf. Table I). (a) Photograph. (b) Differential phase shift $\Delta\varphi$ as a function of frequency (— theory, + measurements). (c) Input reflection coefficient.

$D = 3.82$ mm). This is to compensate for the thickness of the adhesive of about 0.1 mm by which the dielectric was fastened to the waveguide sidewalls. The measured results (Fig. 9(b) and (c)) show good agreement with the theory. The slightly poorer input reflection coefficient measured results from a little gap at the end of the dielectric.

IV. Conclusion

Double dielectric-slab-filled waveguide phase shifters achieve low input reflection behavior (typically less than -30 dB) if the dielectrics are positioned at the sidewalls of the waveguide where the TE_{n0} wave electrical field intensity is low, and linearly tapered matching sections are provided over the entire length. This is demonstrated by exact field theory designs of phase shifters with a 90° differential phase shift at midband from WR 90- through WR 28- (*X*- through *Ka*-) band. The phase error is typically $\pm 4°$ with ± 5-percent frequency variation around the center frequency. If the differential phase compensation effect of the dispersive behavior of the dielectric-filled and empty reference waveguide is utilized, the phase error may be reduced to only $\pm 1°$ within ± 8.5-percent frequency variation. A 90° phase shifter composed of three 30° phase shifters illustrates that the design examples given in the tables may also be used to compose cumulated overall phase shift. Although preferably designed for fixed phase shift, lateral displacement of the tapered dielectric slabs provides a mechanically variable phase shift over a large range. An experimental phase shifter for a 90° midband phase shift at a 14-GHz midband frequency shows good agreement between theory and measurements.

APPENDIX

Matrix Equation, which Results from Field Matching along the Five-Layer Structure of Fig. 2(b) using (1)–(3):

$$(G)\cdot\left(V_n^{(\mathrm{II})}, V_n^{(\mathrm{III})}, W_n^{(\mathrm{III})}, V_n^{(\mathrm{IV})}, W_n^{(\mathrm{IV})}, V_n^{(\mathrm{V})}, W_n^{(\mathrm{V})}, V_n^{(\mathrm{VI})}\right)^T = 0$$

where (G) is given by

$$(G) = \begin{bmatrix}
\sin(k_{xn}^{(\mathrm{II})}c) & -\cos(k_{xn}^{(\mathrm{III})}c) & -\sin(k_{xn}^{(\mathrm{III})}c) & 0 \\
0 & \cos(k_{xn}^{(\mathrm{III})}d) & \sin(k_{xn}^{(\mathrm{III})}d) & -\cos(k_{xn}^{(\mathrm{IV})}d) \\
0 & 0 & 0 & \cos(k_{xn}^{(\mathrm{IV})}e) \\
0 & 0 & 0 & 0 \\
\cos(k_{xn}^{(\mathrm{II})}c)k_{xn}^{(\mathrm{II})} & \sin(k_{xn}^{(\mathrm{III})}c)k_{xn}^{(\mathrm{III})} & -\cos(k_{xn}^{(\mathrm{III})}c)k_{xn}^{(\mathrm{III})} & 0 \\
0 & -\sin(k_{xn}^{(\mathrm{III})}d)k_{xn}^{(\mathrm{III})} & \cos(k_{xn}^{(\mathrm{III})}d)k_{xn}^{(\mathrm{III})} & \sin(k_{xn}^{(\mathrm{IV})}d)k_{xn}^{(\mathrm{IV})} \\
0 & 0 & 0 & -\sin(k_{xn}^{(\mathrm{IV})}e)k_{xn}^{(\mathrm{IV})} \\
0 & 0 & 0 & 0
\end{bmatrix}$$

$$\begin{bmatrix}
0 & 0 & 0 & 0 \\
-\sin(k_{xn}^{(\mathrm{IV})}d) & 0 & 0 & 0 \\
\sin(k_{xn}^{(\mathrm{IV})}e) & -\cos(k_{xn}^{(\mathrm{V})}e) & -\sin(k_{xn}^{(\mathrm{V})}e) & 0 \\
0 & \cos(k_{xn}^{(\mathrm{V})}f) & \sin(k_{xn}^{(\mathrm{V})}f) & -[\sin(k_{xn}^{(\mathrm{VI})}f)-\tan(k_{xn}^{(\mathrm{VI})}a)\cos(k_{xn}^{(\mathrm{VI})}f)] \\
0 & 0 & 0 & 0 \\
-\cos(k_{xn}^{(\mathrm{IV})}d)k_{xn}^{(\mathrm{IV})} & 0 & 0 & 0 \\
\cos(k_{xn}^{(\mathrm{IV})}e)k_{xn}^{(\mathrm{IV})} & \sin(k_{xn}^{(\mathrm{V})}e)k_{xn}^{(\mathrm{V})} & -\cos(k_{xn}^{(\mathrm{V})}e)k_{xn}^{(\mathrm{V})} & 0 \\
0 & -\sin(k_{xn}^{(\mathrm{V})}f)k_{xn}^{(\mathrm{V})} & \cos(k_{xn}^{(\mathrm{V})}f)k_{xn}^{(\mathrm{V})} & -[\cos(k_{xn}^{(\mathrm{VI})}f)+\tan(k_{xn}^{(\mathrm{VI})}a)\sin(k_{xn}^{(\mathrm{VI})}f)]k_{xn}^{(\mathrm{VI})}
\end{bmatrix} \quad \text{(A1)}$$

where T is the transposed vector.

Coupling Integrals in (7) and (8):

$$I_{1nm}^{(\mathrm{II})} = \int_0^c \sin\left(k_{xm}^{(\mathrm{II})}x\right)\sin\left(\frac{n\pi}{a}x\right)dx$$

$$I_{1nm}^{(\mathrm{III})} = \int_c^d \cos\left(k_{xm}^{(\mathrm{III})}x\right)\sin\left(\frac{n\pi}{a}x\right)dx$$

$$I_{2nm}^{(\mathrm{III})} = \int_c^d \sin\left(k_{xm}^{(\mathrm{III})}x\right)\sin\left(\frac{n\pi}{a}x\right)dx$$

$$I_{1nm}^{(\mathrm{IV})} = \int_d^e \cos\left(k_{xm}^{(\mathrm{IV})}x\right)\sin\left(\frac{n\pi}{a}x\right)dx$$

$$I_{2nm}^{(\mathrm{IV})} = \int_d^e \sin\left(k_{xm}^{(\mathrm{IV})}x\right)\sin\left(\frac{n\pi}{a}x\right)dx$$

$$I_{1nm}^{(\mathrm{V})} = \int_e^f \cos\left(k_{xm}^{(\mathrm{V})}x\right)\sin\left(\frac{n\pi}{a}x\right)dx$$

$$I_{2nm}^{(\mathrm{V})} = \int_e^f \sin\left(k_{xm}^{(\mathrm{V})}x\right)\sin\left(\frac{n\pi}{a}x\right)dx$$

$$I_{1nm}^{(\mathrm{VI})} = \int_f^a \sin\left(k_{xm}^{(\mathrm{VI})}x\right)\sin\left(\frac{n\pi}{a}x\right)dx$$

$$I_{2nm}^{(\mathrm{VI})} = \int_f^a \tan\left(k_{xm}^{(\mathrm{VI})}a\right)\cos\left(k_{xm}^{(\mathrm{VI})}x\right)\sin\left(\frac{n\pi}{a}x\right)dx. \quad \text{(A2)}$$

Scattering Coefficients in (8):

$$\begin{aligned}
(S_{11}) &= 2(N_H)^{-1}(M_H) \\
&\quad\cdot\left[(N_E)^{-1}(M_E)+(N_H)^{-1}(M_H)\right]^{-1}-(U) \\
(S_{12}) &= 2(N_H)^{-1}(M_H) \\
&\quad\cdot\left[(N_E)^{-1}(M_E)+(N_H)^{-1}(M_H)\right]^{-1}(N_E)^{-1}(M_E) \\
(S_{21}) &= 2\left[(N_E)^{-1}(M_E)+(N_H)^{-1}(M_H)\right]^{-1} \\
(S_{22}) &= 2\left[(N_E)^{-1}(M_E)+(N_H)^{-1}(M_H)\right]^{-1} \\
&\quad\cdot(N_E)^{-1}(M_E)-(U) \quad \text{(A3)}
\end{aligned}$$

where (U) is the unity matrix; the diagonal matrices (N_H), (N_E), and matrices (M_H), (M_E) are given by (6) and (7). The amplitude coefficients $V_i\mathrm{m}^{(\mathrm{III})},\cdots, V_m^{(\mathrm{IV})}, W_m^{(\mathrm{III})},\cdots, W_m^{(\mathrm{V})}$, in (6) and (7) are expressed by the amplitude coefficient $V_m^{(\mathrm{II})}$ using (A1). The quotient $(V_n^{(\mathrm{I})})/(V_m^{(\mathrm{II})})$, which then still remains in (6) and (7), is suitably normalized so [2] that the power carried by a given wave is 1 W for a wave-amplitude coefficient A_n, B_m of $\sqrt{1\ \mathrm{W}}$:

$$1 = \frac{\left(V_m^{(\mathrm{II})}\right)^2\cdot\sum_{r=\mathrm{II}}^{\mathrm{VI}}\left[\frac{1}{2}\,\mathrm{Re}\iint_{\mathrm{Area}(r)}(\vec{E}^{(s)}\times\vec{H}^{(s)*})\,d(\mathrm{Area}(r))\right]}{\left(V_n^{(\mathrm{I})}\right)^2\cdot\frac{1}{2}\,\mathrm{Re}\iint_{\mathrm{Area(I)}}(\vec{E}^{(I)}\times\vec{H}^{(I)*})\,d(\mathrm{Area}(I))} \quad \text{(A4)}$$

where $r = \text{II}, \cdots, \text{VI}$; the integrals are between the limits of the corresponding cross-section area of the empty section I, and the five-layer structure II, $\cdots$, VI.

Scattering Coefficients for Two Series-Connected Structures with the Scattering Matrices $(S)^{(1)}$ and $(S)^{(2)}$:

$$(S_{11})^{(\text{total})} = (S_{11})^{(1)} + (S_{12})^{(1)}\left[(U) - (S_{11})^{(2)}(S_{22})^{(1)}\right]^{-1} \cdot (S_{11})^{(2)}(S_{21})^{(1)}$$

$$(S_{12})^{(\text{total})} = (S_{12})^{(1)}\left[(U) - (S_{11})^{(2)}(S_{22})^{(1)}\right]^{-1}(S_{12})^{(2)}$$

$$(S_{21})^{(\text{total})} = (S_{21})^{(2)}\left[(U) - (S_{22})^{(1)}(S_{11})^{(2)}\right]^{-1}(S_{21})^{(1)}$$

$$(S_{22})^{(\text{total})} = (S_{21})^{(2)}\left[(U) - (S_{22})^{(1)}(S_{11})^{(2)}\right]^{-1} \cdot (S_{22})^{(1)}(S_{12})^{(2)} + (S_{22})^{(2)} \quad \text{(A5)}$$

where (U) is the unity matrix.

REFERENCES

[1] N. Marcuvitz, *Waveguide Handbook*. New York: McGraw-Hill, 1951, pp. 224–248.

[2] R. E. Collin, *Field Theory of Guided Waves*. New York: McGraw-Hill, 1960, pp. 224–247, 85–87, 174–179.

[3] R. E. Collin, *Foundations for Microwave Engineering*. New York: McGraw-Hill, 1966.

[4] F. E. Gardiol, "Higher order modes in dielectrically loaded rectangular waveguides," *IEEE Trans. Microwave Theory Tech.*, vol. MTT-16, pp. 919–924, Nov. 1968.

[5] G. N. Tsandoulas, D. H. Temme, and F. G. Willwerth, "Longitudinal section mode analysis of dielectrically loaded rectangular waveguides with application to phase shifter design," *IEEE Trans. Microwave Theory Tech.*, vol. MTT-18, pp. 88–95, Feb. 1970.

[6] C. T. Liu and C. H. Chen, "A variational theory for wave propagation in inhomogeneous dielectric slab loaded waveguides," *IEEE Trans. Microwave Theory Tech.*, vol. MTT-29, pp. 805–812, Aug. 1981.

[7] C. T. M. Chang, "Partially dielectric slab-filled waveguide phase shifter," *IEEE Trans. Microwave Theory Tech.*, vol. MTT-22, pp. 481–485, May 1974.

[8] F. Arndt, J. Bornemann, and R. Vahldieck, "Design of multisection impedance matched dielectric-slab filled waveguide phase shifters," *IEEE Trans. Microwave Theory Tech.*, vol. MTT-32, pp. 34–39, Jan. 1984.

[9] A. J. Simmons, "Phase shift by periodic loading of waveguide and its application to broad-band circular polarization," *IRE Trans. Microwave Theory Tech.*, vol. MTT-3, pp. 18–21, Dec. 1955.

[10] R. F. Harrington, *Time Harmonic Electromagnetic Fields*. New York: McGraw-Hill, 1961, pp. 171–177.

[11] H. Patzelt and F. Arndt, "Double plane steps in rectangular waveguides and their application for transformers, irises, and filters," *IEEE Trans. Microwave Theory Tech.*, vol. MTT-30, pp. 770–776, May 1982.

[12] F. Arndt, U. Tucholke, and T. Wriedt, "Broadband dual-depth *E*-plane corrugated square waveguide polarizer," *Electron. Lett.*, vol. 20, pp. 458–459, May 1984.

[13] R. Levy, "A high-power *X*-band Butler matrix," *Microwave J.*, vol. 27, pp. 135–141, Apr. 1984.

Fritz Arndt (SM'83) was born in Konstanz, Germany, on April 30, 1938. He received the Dipl.-Ing., the Dr.-Ing., and the Habilitation degrees from the Technical University of Darmstadt, Germany, in 1963, 1968, and 1972, respectively.

From 1963 to 1972, he worked on directional couplers and microstrip techniques at the Technical University of Darmstadt. Since 1972, he has been a Professor and Head of the Microwave Department at the University of Bremen, Germany. His research activities are, at present, in the area of the solution of field problems of waveguide, finline and optical waveguide structures, of antenna design, and of scattering structures.

Dr. Arndt is member of the VDE and NTG (Germany). In 1970, he received the NTG award, and in 1982 the A. F. Bulgin Award (together with three coauthors) from the Institution of Radio and Electronic Engineers.

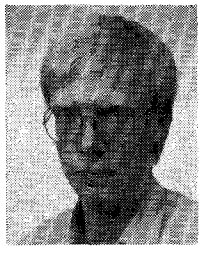

Andreas Frye was born in Steinfeld/Oldenburg, Germany, on June 21, 1959. He received the Dipl.-Ing. degree in electrical engineering from the University of Bremen, Germany, in 1983.

Since 1983, he has worked in the Department of Theoretical Electrotechnics of the University of Bremen on the theory of electromagnetic fields influenced by moved matter.

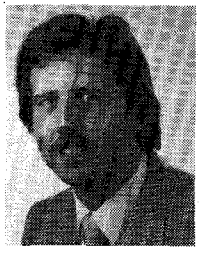

Manfred Wellnitz was born in Schiffdorf/Bremerhaven, Germany, on December 18, 1957. He studied at the Technical University of Braunschweig and the University of Bremen. He received the Dipl.-Ing. degree in electrical engineering from the University of Bremen, Germany, in 1983.

Rainer Wirsing was born on September 22, 1957, in Hannover. He finished school in 1976 and started to study electric engineering at the University of Bremen. He took his degree in 1983.

At the present, he is employed at Philips in Bremen. He is occupied in the development of software.